

Adsorption and kinetic effects on crack growth in MnZn ferrites

M.A.H. Donners^{a)}

*Laboratory of Solid State and Materials Chemistry, Eindhoven University of Technology,
P.O. Box 513, 5600 MB, Eindhoven, The Netherlands*

L.J.M.G. Dortmans

TNO Institute of Applied Physics, P.O. Box 595, 5600 AN, Eindhoven, The Netherlands

G. de With^{b)}

*Laboratory of Solid State and Materials Chemistry, Eindhoven University of Technology,
P.O. Box 513, 5600 MB, Eindhoven, The Netherlands*

(Received 21 September 1999; accepted 27 March 2000)

The variation of the fracture toughness of MnZn ferrite ceramics with varying loading rate and humidity was determined with the aid of the single edge notched beam (SENB) test. A strong decrease with increasing humidity and decreasing loading rate was observed. A model for subcritical crack growth incorporating kinetic and adsorption effects was formulated to analyze the data. The value of the adsorption-controlled fracture toughness was determined independently by double torsion experiments and agreed favorably with the values as determined from the SENB data using the model. The strength of the material was determined, and analysis showed a strength behavior similar to the fracture toughness behavior, as predicted by the model. The analysis presented can be used to assess the subcritical crack growth behavior using a limited number of SENB specimens.

I. INTRODUCTION

Thanks to their ferrimagnetic properties, combined with a high electric resistivity, MnZn ferrites find many applications; for example, in power transformers and filters, which are used in many consumer, communications, and automotive products. For many of these applications, it is expected that in the near future the ferrites will be exposed to higher mechanical stresses. This is caused by an increase in power throughput, combined with miniaturization, leading to higher power losses relative to the size of the component; by automated printed circuit board mounting and soldering; or by mechanical vibrations as found in the growing field of automotive applications. This has quite recently brought about an interest in the mechanical reliability of ferrites. MnZn ferrites obey linear elastic fracture mechanics, controlled by defects generally caused by processing, machining, or handling steps. One of the important material parameters to be determined is the fracture toughness. It relates the size of the defects present and the resulting strength of a body. An important aspect of the mechanical behavior of MnZn ferrites is the influence humidity has on their strength, as shown in earlier work.¹ The usual explana-

tion for this phenomenon is subcritical crack growth (SCG), whereby in the presence of a reactive species, a crack can grow at stresses below the critical value determined from the fracture toughness. In this paper, it will be shown that measurement of the fracture toughness of an SCG-susceptible material is possible, but that the analysis of the experiments has to account for subcritical crack extension. If such an adaptation is made, certain fracture toughness tests can even be used to determine the SCG behavior of a material, with considerably less effort compared to using series of strength measurements because of the smaller number of specimens required.

Most types of fracture toughness tests are based on performing a strength test on a specimen with an artificial defect of known dimensions. These defects are made significantly larger than the "naturally" occurring defects. In this way, the test piece is practically certain to fail on the artificial defect. Usually, a crack is introduced in the material by indentation; or a notch, continuous over the thickness of the specimen, is cut using a diamond saw. In single edge notched beam (SENB) tests, these are straight. The notched bar is then subjected to a four-point bending test, to measure the fracture force. If the material to be tested is susceptible to SCG, the fracture force will vary with the loading rate. The "inert" fracture toughness can be measured at very high loading rates or very low humidities. This parameter can also be determined by extrapolating the fracture toughness as

^{a)}Present address: Philips Center for Manufacturing Technologies, P.O. Box 218, 5600 MD, Eindhoven, The Netherlands.

^{b)}Address all correspondence to this author.

measured at several loading rates. In many other fracture toughness tests (e.g., the Chevron notch test), one can only use relatively low load rates, which makes them inappropriate for use with SCG-susceptible materials. In the analysis of fracture toughness tests, it is commonly assumed that the notch depth equals the critical defect size, assuming explicitly that no subcritical crack growth occurs.

This paper tries to answer two questions. First, how can the influence of the environmental humidity on the fracture toughness be accounted for when using a standard fracture toughness test, as in this case, the SENB method. Second, could these tests combined with the SCG model proposed here be used to characterize the susceptibility of the material to the effects of humidity? In the following sections, the results of the SENB specimens are discussed, employing the SCG analysis. Finally, the available strength data will be compared with the fracture toughness data.

Energetic crack extension criteria

At equilibrium according to Griffith,

$$G_I = G_{Ic} = \frac{K_{Ic}^2}{E'} = R \quad (1)$$

For values of the mechanical energy release rate, G_I , larger than the critical value, here denoted as fracture energy, R , the crack will extend. Here E' denotes the relevant elastic modulus. For MnZn ferrites, R is assumed to be independent of crack length, although for some materials R is known to increase with increasing crack length. Ideally, extending a crack in a body B with fracture surface energy γ_B in a vacuum results in

$$R_0 = 2\gamma_B \quad (2)$$

The critical stress intensity or “fracture toughness” can be used as a criterion for crack extension. For mode I, the fracture stress of a body, σ_f , is determined by a combination of the critical stress intensity or fracture toughness, K_{Ic} , and the critical defect size, c_c ,

$$\sigma_f = \frac{K_{Ic}}{Y\sqrt{c_c}} = \frac{\sqrt{E'R}}{Y\sqrt{c_c}} \quad (3)$$

where Y is a geometric factor. Equation (3) shows that the strength of a material can decrease in two ways.

First, the fracture toughness can be decreased by decreasing the fracture surface energy. This effect can be brought about by introducing an adsorbing species in the environment. For mode I, loading in vacuum of a body containing a defect of initial size c_i , the inert fracture toughness, \tilde{K}_{Ic} , is given by

$$\tilde{K}_{Ic} = Y\tilde{\sigma}_f\sqrt{c_i} \quad (4)$$

using the “inert” strength, $\tilde{\sigma}_f$. It is often assumed that the fracture toughness is a materials constant. Adsorption of

a gas or vapor on the fracture surface, however, will decrease the fracture surface energy and, therefore, R . In that case, the fracture toughness is reduced to the adsorption-controlled fracture toughness,

$$\tilde{K}_{Ic} = Y\tilde{\sigma}_f\sqrt{c_i} = \sqrt{E'R_0} \quad (5)$$

introducing the adsorption controlled strength, $\hat{\sigma}_f$.

Second, the crack can extend to $c > c_i$ at stress intensities well below the critical value K_{Ic} , by the action of a reactive species. By the formation of a transition state complex, the activation energy for crack extension can be decreased. In that case, the actual strength is decreased to $\sigma_f < \tilde{\sigma}_f$. The fracture toughness is in that case formulated as

$$\tilde{K}_{Ic} = Y\sigma_f\sqrt{c_c} \quad (6)$$

using the critical crack length c_c . This effect is called subcritical or slow crack growth, usually abbreviated SCG.

Both effects can act simultaneously, resulting in

$$\hat{K}_{Ic} = Y\sigma_f\sqrt{c_c} \quad (7)$$

This combined mechanism will be treated theoretically and its applicability to the experimental data will be checked. To be able to determine the dependence of the fracture toughness on adsorption effects, Sec. II gives a detailed discussion on adsorption and its effects on surface energy. Section III will deal with the description of subcritical crack growth based on chemical reaction kinetics, combined with the adsorption effect. Finally, the resulting considerations will be applied to the analysis of fracture toughness and strength experiments.

II. ADSORPTION

In general, gas or vapor molecules can adsorb as one molecule or by splitting up in several parts. This is called nondissociative and dissociative adsorption. Some adsorbates can react according to both mechanisms. In practice, more than one adsorbate is likely to be present. In this section, the adsorption resulting from these mechanisms and from some of their combinations will be described. The nondissociative adsorption of water vapor will be described using the Langmuir isotherm for adsorption,²

$$\theta_{X,n} = \frac{b_{X,n}p_X}{1 + b_{X,n}p_X} \quad (8)$$

where $\theta_{X,n}$ is the relative surface coverage by nondissociative adsorption, $b_{X,n}$ is the relevant Langmuir parameter, and p_X is the relative partial pressure.

The effect of adsorption on fracture energy

Introduction of an adsorbing species, X, in the environment will decrease the fracture energy in vacuum, R_0 ($= 2\gamma_B$), to

$$R_X = R_0 - 2\Delta U_{ad} = 2\gamma_{BX} \quad (9)$$

using γ_{BX} , the energy to form one unit area of interface B–X, relative to the initial B–B state and using the adsorption energy ΔU_{ad} . The latter can be calculated using the Gibbs adsorption equation³

$$\frac{d(\Delta U_{ad})}{d[\ln(a_X)]} = k_B T \Gamma(a_X) \quad (10)$$

using Γ , the excess concentration of environmental species X at the B–X interface; a_X , the chemical activity of that species; and where k_B and T denote Boltzmann’s constant and temperature, respectively. If the adsorption isotherm, $\Gamma(p_X)$, is known and is continuously increasing with p_X , the adsorption energy can be calculated from Eq. (10) as

$$\Delta U_{ad} = k_B T \Gamma_M \int_0^{p_X} \frac{\theta_X}{p_X} dp_X \quad (11)$$

using the Langmuir adsorption isotherm [Eq. (8)] and the excess at full coverage, Γ_M . This equation results in a dependence of R_X on p_X , given by

$$R_X = R_0 - 2\Gamma_M k_B T \ln(1 + bp_X) \quad (12)$$

Introducing this into the Griffith equilibrium [Eq. (1)] results in

$$\hat{K}_{Ic} = \tilde{K}_{Ic} \sqrt{1 - \Phi \ln(1 + bp_X)} \quad (13)$$

The constant Φ ,

$$\Phi = \frac{2\Gamma_M k_B T}{R_0} \quad (14)$$

determines the ratio of the energy released by adsorption to the fracture energy dissipated by crack growth, both per unit area. High Γ_M and b will result in a considerable decrease in fracture toughness. High values of R_0 will cause the material to be relatively less sensitive to the effect of adsorption. However, increasing R_0 can also change the adsorption affinity.

III. SUBCRITICAL CRACK GROWTH

Many materials show a lower strength in the presence of reactive species in the environment. The most frequently used term for this effect is subcritical crack growth. In this section, the possible effects of the reactive environment on the mechanical reliability of MnZn ferrites will be discussed.

Chemical reaction rate and adsorption model

An SCG-promoting species can act in two ways. On the one hand, it can decrease the surface energy by covering the fresh fracture surface. In Fig. 1, this reaction mechanism is shown by states I–IIa–IIIa–IV. On the other hand, a reactive molecule can form a transition state complex with the stressed bond at the crack tip, effectively decreasing the amount of energy needed to break this bond. This mechanism corresponds to states I–IIb–IIIb–IV.

If crack growth is seen as a molecular reaction between a reactive species with relative partial pressure p_X and a solid surface, the reaction or crack growth rate can be approximated by the rate of the rate-determining reaction step, which is, according to the classical theory of rate processes, given by⁴⁻⁷

$$v = p_X^\eta l_0 \frac{kT}{h} \left[\exp\left(-\frac{\Delta U_F}{kT}\right) - \exp\left(-\frac{\Delta U_B}{kT}\right) \right] \quad (15)$$

using a characteristic crack growth step length, l_0 ; the (pseudo-) reaction order of p_X , η ; and the molecular free energies of formation of a transition state complex in a forward and backward reaction, ΔU_F and ΔU_B , respectively. These energies can be substituted according to

$$v = p_X^\eta l_0 \frac{kT}{h} \left[\exp\left(-\frac{U_F - \alpha(G - R_X)}{kT}\right) - \exp\left(-\frac{U_B + \alpha(G - R_X)}{kT}\right) \right] \quad (16)$$

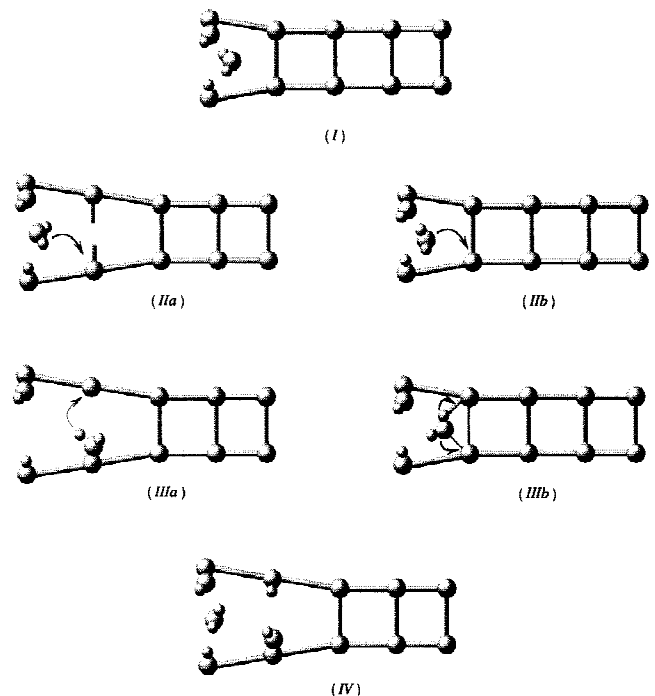


FIG. 1. Atomistic representation of two possible bond-breaking mechanisms.

using the activation area, α , and the activation energies for bond rupture and bond healing, U_F and U_B , respectively. The mechanical energy applied to the system is accounted for by the mechanical energy release rate, G , and the surface energy effects are accounted for by the adsorption-dependent work of fracture, R_X [Eq. (12)]. The effects of these factors on the activation energies is shown in Fig. 2.

Usually, the backward reaction is neglected, which simplifies the rate equation to

$$v = v_0 p_X^\eta \exp\left[\frac{\alpha(G - R_X)}{kT}\right], \quad (17)$$

with the pre-exponential factor given by

$$v_0 = \frac{kT}{h} l_0 \exp\left(-\frac{U_F}{kT}\right). \quad (18)$$

With Eq. (1),

$$G = \frac{K_I^2}{E'}, \quad (19)$$

and Eqs. (12) and (13), the driving force for crack extension can be written as

$$G - R_X = R_0 \left[\frac{K_I^2}{\hat{K}_{Ic}^2} - 1 + \Phi \ln(1 + bp_X) \right]. \quad (20)$$

This modifies the rate equation to

$$v = v_0 p_X^\eta \exp\left[-\beta \left(1 - \frac{K_I^2}{\hat{K}_{Ic}^2}\right)\right] (1 + bp_X)^{\beta\Phi}, \quad (21)$$

using the constant β given by

$$\beta = \frac{\alpha R_0}{kT}. \quad (22)$$

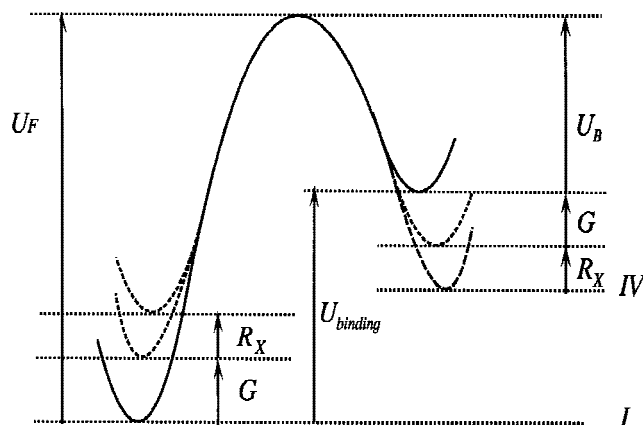


FIG. 2. Potential energy levels of different states in bond-breaking mechanism.

For values of the stress intensity that are small relative to the inert fracture toughness and large values of β , Eq. (21) can be simplified to

$$v = v_0 p_X^\eta \left(\frac{K_I}{\hat{K}_{Ic}}\right)^n (1 + bp_X)^{n\Phi/2}, \quad (23)$$

as

$$\exp(-ax) \approx (1 - x)^a, \quad (24)$$

for small values of x and large values of a . The SCG constant, n , is given by

$$n = 2\beta. \quad (25)$$

For subsequent analyses, Eq. (23) can be written more conveniently as

$$v = v_{pX} \left(\frac{K_I}{\hat{K}_{Ic}}\right)^n, \quad (26)$$

with the adsorption-controlled fracture toughness, \hat{K}_{Ic} , and the pre-exponential factor

$$v_{pX} = v_\eta v_{ads} \sqrt{1 - \Phi \ln(1 + bp_X)^n}, \quad (27)$$

using a factor, v_{ads} , accounting for the effect of adsorption,

$$v_{ads} = (1 + bp_X)^{n\Phi/2}, \quad (28)$$

and a factor accounting for the reaction kinetics effect,

$$v_\eta = v_0 p_X^\eta. \quad (29)$$

IV. THE ANALYSIS OF FRACTURE TOUGHNESS TESTS

A. Single edge notched beam tests

The apparent or nominal fracture toughness as determined by SENB experiments, neglecting the effect of SCG, is given by⁸

$$K_{IcS} = F_f \frac{3(l_1 - l_2)}{2wh^2} Y_S \sqrt{c_0}, \quad (30)$$

using the fracture force, F_f , and using the relevant sizes of the specimen. The latter include the beam width, w , the beam height, h , and the outer and inner spans, l_1 and l_2 , respectively. The defect geometry factor, Y_S , can be given by the Gross–Srawley relation as⁹

$$Y_S = 1.99 - 2.47\alpha + 12.97\alpha^2 - 23.17\alpha^3 + 24.8\alpha^4, \quad (31)$$

which is valid for $0 \leq \alpha \leq 0.6$ and $l/h \approx 8$, using the relative notch depth, α , depending on the notch depth, c , and the specimen height, h ,

$$\alpha = \frac{c}{h} \quad (32)$$

This function has a minimum around $\alpha = 0.15$. The notch depth machined in the SENB specimens is chosen around this value. As the crack is not expected to double its length by SCG and Y_S is approximately constant in the range c_1 to $2c_1$, the parameter Y_S can safely be assumed to remain constant at its initial value.

B. The effects of SCG in SENB tests

In the standard analysis of SENB tests, it is assumed that the critical defect size equals the notch depth as machined, c_0 . However, if the material to be tested is susceptible to subcritical crack growth and relatively low stress rates are applied, the crack is likely to extend before catastrophic failure. Ignoring this effect will cause the fracture toughness to be underestimated, as the defect size at the moment of failure has become larger than the original notch depth.

Substituting Eq. (30) for K_I in the SCG power law, Eq. (26) results in

$$\frac{dc}{dt} = \frac{v_{px} g_S^n \dot{F}^n}{\hat{K}_{Ic}^n} Y_S^n (c) t^n \sqrt{c^n} \quad (33)$$

using the load given as a function of time t as $F = \dot{F} \cdot t$, with $\dot{F} = dF/dt$. The SENB test geometry factor, g_S , is defined as

$$g_S = \frac{3(l_1 - l_2)}{2wh^2} \quad (34)$$

Using

$$\dot{F}^n t^{n+1} = \frac{F_f^{n+1}}{\dot{F}} \quad (35)$$

this results in

$$\int_{c_0}^{c_c} \frac{dc}{Y_S^n (c) \sqrt{c^n}} = \frac{1}{n+1} \frac{v_{px} g_S^n F_f^{n+1}}{\hat{K}_{Ic}^n \dot{F}} \quad (36)$$

From this expression, the fracture force can be isolated, giving

$$F_f = \left[\frac{(n+1) \dot{F} \hat{K}_{Ic}^n}{g_S^n v_{px}} \int_{c_0}^{c_c} \frac{dc}{Y_S^n (c) \sqrt{c^n}} \right]^{1/(n+1)} \quad (37)$$

Now we can introduce the assumption that the compliance factor, Y_S , is independent of the crack length and is

kept constant at the value determined for the initial notch depth, c_0 . In that case, the integral can be evaluated analytically. Using the apparent fracture toughness,

$$K_{IcS} = Y_S g_S F_f \sqrt{c_0} \quad (38)$$

and the adsorption-controlled fracture toughness,

$$\hat{K}_{Ic} = Y_S g_S F_f \sqrt{c_c} \quad (39)$$

results in

$$\frac{K_{IcS}}{\hat{K}_{IcS}} = \sqrt[2-n]{1 + \frac{n-2}{2(n+1)} \frac{v_{px} g_S^2 Y_S^2 F_f^3}{\hat{K}_{Ic}^2 \dot{F}}} \quad (40)$$

which shows that the value for fracture toughness resulting from a standard analysis will be underestimated at lower load rates. The last step is to substitute Eq. (38) for the actual fracture toughness, which gives

$$F_f = \frac{\hat{K}_{Ic}}{Y_g \sqrt{c_0}} \left[1 + \frac{n-2}{2(n+1)} \frac{v_{px} g_S^2 Y_S^2 F_f^3}{\hat{K}_{Ic}^2 \dot{F}} \right]^{1/(2-n)} \quad (41)$$

C. Correspondence between strength and fracture toughness

Starting from Eq. (40), if the apparent fracture toughness is small with respect to the adsorption-controlled fracture toughness, the apparent fracture toughness can be formulated as

$$K_{IcS} = \left[\frac{2(n+1) Y_S g_S \dot{F}}{n-2} \frac{\sqrt{c_0^3 \hat{K}_{Ic}^n}}{v_{px}} \right]^{1/(n+1)} \quad (42)$$

using the initial defect size, c_0 , and the geometry factor, Y_S , of the SENB specimen.

For the strength tests, in a similar way, using the initial defect size, c_i , and the geometry factor, Y , both of the strength specimen, and using Eqs. (38) and (39) and

$$\hat{K}_{Ic} = Y g \hat{F}_f \sqrt{c_c} \quad (43)$$

the strength of a specimen can be expressed as

$$\sigma_f = \left[\frac{2(n+1) g \dot{F}}{n-2} \frac{\hat{K}_{Ic}^n}{v_{px} Y^n \sqrt{c_i^{n-2}}} \right]^{1/(n+1)} \quad (44)$$

if the apparent fracture strength is small with respect to the adsorption-controlled fracture strength. If both the actual fracture toughness and the actual strength are known for a combination of loading rate and humidity, their ratio can be calculated:

$$\frac{K_{IcS}}{\sigma_f} = Y \sqrt{c_i} \left(\frac{Y_S \sqrt{c_0^3}}{Y \sqrt{c_i^3}} \right)^{1/(n+1)} \quad (45)$$

assuming that the test geometry factors, g_S and g , are about equal. If this ratio is a constant for all combinations of humidity and loading rate, this means that the susceptibility to the effects of humidity is a property of the material, independent from the type or geometry of defect or specimen. It also implies that the effect of humidity, whether subcritical crack growth, or an adsorption effect, or a combination of both, manifests itself in the same way in both strength and SENB fracture toughness tests, making the latter appropriate to characterize the effects of humidity on crack growth.

V. ANALYSIS OF DOUBLE TORSION TESTS

In Eq. (46) F denotes the force, h and h_n the thickness and thickness in the groove, w and w_m the width of the specimen and loading span, and ν Poisson's ratio ($\nu = 0.30$). The stress intensity of a double torsion (DT) specimen is given by¹⁰

$$K_I = Fw_m \sqrt{\frac{3}{wh^3h_n(1-\nu)\psi(\tau)}}, \quad (46)$$

correcting for finite beam thickness with a factor $\psi(\tau)$. The parameter τ is given by

$$\tau = \frac{2h}{w}. \quad (47)$$

For values of τ smaller than 1 (square cross section of the beams), ψ can be approximated by¹¹

$$\psi(\tau) = 1 - 0.6302\tau + 1.20\tau \cdot e^{-\pi/\tau}, \quad (48)$$

with an accuracy of better than 0.1%. Note that the stress intensity is independent of the crack length. In practice this only applies in the mid 60% to 70% of the specimen length.^{11–13}

The fracture toughness can be measured by applying a force causing direct catastrophic fracture, F_f .^{13–15} If the initial crack length is sufficiently long, the crack can grow subcritically, without any influence of the crack length on the stress intensity. Only the chemical activity of the reactive species will influence the fracture toughness. In the absence of region II, diffusion limitation to SCG can be neglected. Therefore, in fact, the adsorption-controlled fracture toughness, \hat{K}_{Ic} , is determined by this method as a function of the environmental humidity, instead of the inert fracture toughness, \tilde{K}_{Ic} . This modifies Eq. (46) to

$$\hat{K}_{Ic} = F_f w_m \sqrt{\frac{3}{wh^3h_n(1-\nu)\psi(\tau)}}. \quad (49)$$

VI. EXPERIMENTAL PROCEDURES

A. Fracture toughness tests

The experiments were performed on two types of MnZn ferrite, labeled type 2 and type 4,² made using standard mixed-oxide processing and resulting in so-

called E 42 cores.² The nominal composition was 71.0 wt% Fe₂O₃, 20.5 wt% MnO, and 8.5 wt% ZnO. The nominal grain size, as determined from the mean intercept length, was 7.3 μm while the density was 4.8 g/cm³, corresponding to a relative density of 94%. For the experiments, bars of 3.5 \times 4.5 \times 42 mm³ without a chamfer were used. The notches were cut to a depth of 15% of the specimen height, in one to three passes, using a diamond saw blade with a width of 100 μm . Further material details are given in Ref. 2.

As the stress applied at the notch must be known as exactly as possible, a four-point test jig with inner and outer spans of 15 and 36 mm, respectively, was used. Typically, five specimens were used for testing. The humidity in the test chamber is set by flushing the chamber surrounding the specimen with dry nitrogen gas or with humidified air. Alternatively, the test is conducted with the bar submerged in water. After this, the bar is loaded with a loading rate of 0.2, 2, or 20 mm min⁻¹, corresponding to 2.3, 26.3, and 275 N s⁻¹, respectively, as was determined experimentally. After the test, the dimensions of the bar and the notch were measured using an electronic micrometer and an optical microscope equipped with a measuring ocular. The tested bars were subsequently subjected to a fractographical analysis to determine whether they failed “regularly” (i.e., no failure initiation from pores or other defects on the notch tip). One series of tests was performed on a four-point bending test machine, mounted in the vacuum chamber of a scanning electron microscope (SEM) at a pressure equal to or lower than 7×10^{-4} Pa, with a loading rate of 9.6 N s⁻¹.

B. Double torsion experiments

Double torsion (DT) specimens measuring nominally 15 \times 42 mm² with a thickness of either 1 or 2 mm were used. The test jig had three lower bearing points, two at the line of loading and one support point near the end of the specimen. A spacer was used for positioning the specimen on the jig. After applying a small preload to fixate the specimen, the spacer was removed from the specimen. The desired test atmosphere humidity was then set by flushing with dry nitrogen or humidified air. To measure the fracture toughness, DT specimens of 1 mm thickness were used with a starting notch length of 14 mm, to ensure that the crack tip, whether the crack grows subcritically or not, is located in the mid 60% of the specimen length. The specimen was positioned and preloaded and the humidity was set, as described above. Then, the specimen was loaded with a constant load rate of 0.2 mm min⁻¹. This low loading rate was chosen to make sure that if subcritical crack growth would occur, the humidity at the crack tip would remain constant, at the same value as in the environment.

As in the standard test, the force was recorded versus time. The load at which catastrophic failure occurred was registered.

C. Strength experiments

The strength of the materials was measured directly using the E-cores with the aid of a modified three-point bend test, the so-called W-test. A span of 36 mm was used with a loading rate of 0.2, 2.0, and 20 mm mm⁻¹, corresponding to 0.470, 8.33, and 84.1 N s⁻¹, respectively. Typically, 25 specimens were used. Before testing, the specimens were chamfered 200 to 300 μm on wet P400 sand paper and subsequently dried. The environment was controlled similarly as in the case of the toughness measurements. Further details are given in Ref. 1.

D. Fractography

Using grid of about 1800 points, the ratio of trans- and intergranular fracture was measured on SEM photographs of the fracture surfaces of the strength specimens, yielding a standard deviation of about 5%. These measurements were done for the three loading rates as used in the strength tests at relative humidities (RH) of 2.5, 60, and (near) 100%. Moreover, the ratio of trans- and intergranular fracture was measured as a function of crack extension at 60% RH at a loading rate of 2.0 mm min⁻¹. Finally, the DT specimens were also examined qualitatively.

VII. RESULTS OF THE VARIOUS TESTS

A. Single edge notched beam test

The results of the SENB tests performed on type-2 and type-4 materials are shown in Figs. 3 and 4. In both cases it is assumed that no subcritical crack growth occurs, which means that the depth of the machined notch is taken as the size of the critical defect. Equation (31) was used to calculate the defect geometry factor, Y_S , for each specimen. The fracture toughness values of the individual bars, calculated using Eq. (30), were averaged over the samples measured at the same load rate and humidity. The standard set size was five. If fractographical analysis raised doubt whether the crack proceeded regularly in a specific sample, it was decided to remove the sample concerned from the set. One set of SENB specimens of 4 type-material was measured in high vacuum ($\leq 7 \times 10^{-4}$ Pa), resulting in a fracture toughness $\tilde{K}_{ICS} = 1.99 \text{ MPa m}^{1/2}$ with a standard deviation of $0.08 \text{ MPa m}^{1/2}$ on the mean. From the literature it is known that under these conditions, the load rate does not influence the fracture toughness of an MnZn ferrite.¹⁶

B. Double torsion tests

The adsorption-controlled fracture toughness, \tilde{K}_{IC} , of type-4 material was determined from the fracture force measured using 1-mm-thick specimens with a 14-mm notch, using Eq. (49). At each humidity, five samples were tested. In some tests, a deflection was found in the load–time curve, as shown in Fig. 5, as opposed to a linear dependence. This (partial) load relaxation is attributed to subcritical crack growth. The tests in which this occurred were replaced by tests in which a linear load–time relationship was found. The mean adsorption-controlled fracture toughness values of the resulting sets are given in Table I.

C. Strength tests

The results of the W-test strength tests performed on type-2 and type-4 materials are shown as ratios of strength over fracture toughness in Figs. 6 and 7. From these graphs we conclude that the behavior of strength and fracture toughness are quite similar.

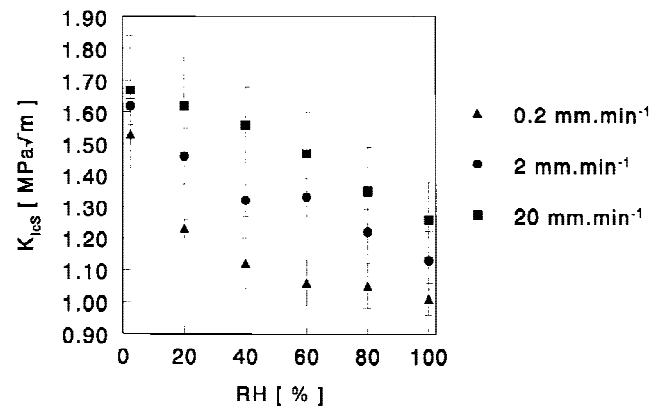


FIG. 3. SENB fracture toughness data of core type 2 at six humidities and three loading rates; error bars indicate standard deviation in the mean.

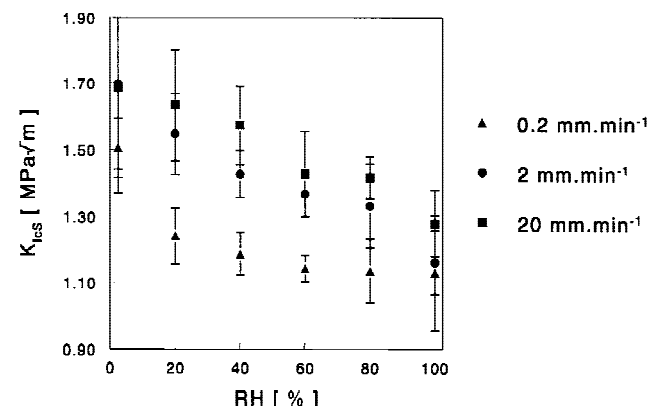


FIG. 4. SENB fracture toughness data of core type 4 at six humidities and three loading rates; error bars indicate standard deviation in the mean.

D. Fractography

From the fractographic analysis of the toughness specimens, only a small effect of loading rate and relative humidity was observed. With higher loading rate and lower relative humidity, a smaller fraction of transgranular fracture was observed but in all cases the fraction transgranular ranged between 60% (high RH, low rate) to 40% (low RH, high rate). The amount of transgranular

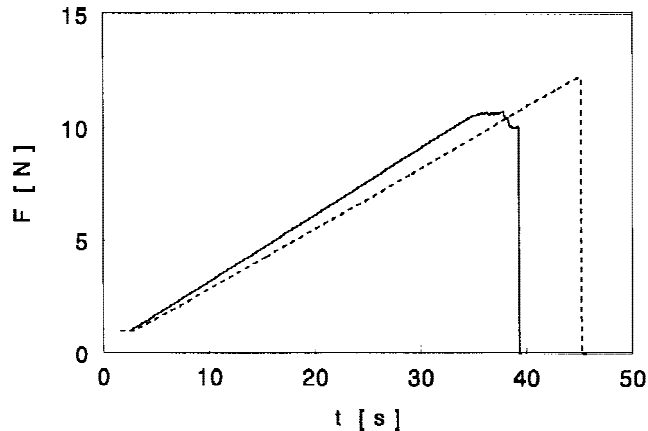


FIG. 5. Load-time curves of DT fracture toughness tests; dashed curve linear until failure and solid curve showing nonlinearity due to subcritical crack extension.

TABLE I. Adsorption-controlled fracture toughness and standard deviation in the mean as measured using DT specimens of type-4 material.

RH (%)	\hat{K}_{Ic} (MPa m ^{1/2})	s.d. \hat{K}_{Ic} (MPa m ^{1/2})
2.5	1.595	0.066
20	1.527	0.130
40	1.393	0.077
60	1.366	0.024
80	1.330	0.083
100	1.194	0.111

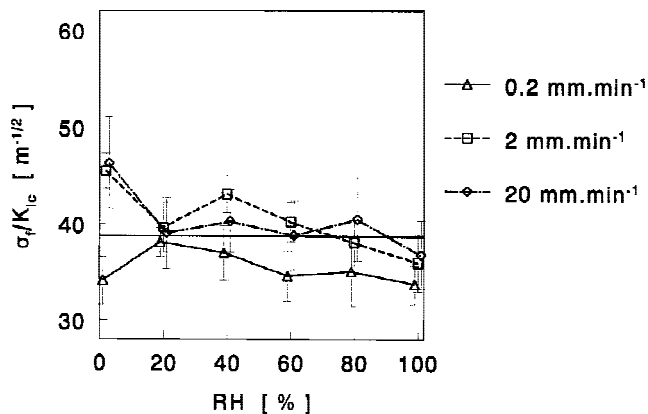


FIG. 6. Value of \mathcal{R} versus relative humidity at three loading rates for type-2 material.

fracture in the strength specimens decreased with crack extension from ~60% at 1 mm from the surface to ~40% at crack extensions larger than 3 mm from the surface. The examination of the DT specimens revealed that crack bridging hardly ever occurred.

VIII. DISCUSSION

A. Double torsion test: Adsorption-controlled fracture toughness

The great advantage of a DT test over an SENB test for measuring the fracture toughness of a material possibly susceptible to subcritical crack growth is that the stress intensity factor of the specimen does not depend on the crack length over the mid 60 to 70% of the specimen length.^{11,12,13} At crack lengths between 20% and 80% of the specimen length, the stress intensity will only depend on the actually applied load. Moreover, subcritical crack growth can easily be observed in a DT specimen. In the literature, the fracture toughness as determined with the DT method has been compared to that measured using flexure specimens.^{15,17} In those cases, a higher fracture toughness was found in the DT test, while in the present case the SENB test results in a higher fracture toughness. This could be caused by measuring the fracture toughness during crack initiation, which would result in higher failure loads.¹⁴ More likely, the discrepancy between the results of the SENB and DT tests can be attributed to the fact that the present DT results were not corrected for the influence of crack shape front, which would increase the fracture toughness in the DT test with 5% to 10%.^{4,23} Unfortunately, the crack front shape could not be determined satisfactorily in the ferrite samples.

B. Analysis using the subcritical crack growth power law

In Fig. 8, the fracture toughness data from Fig. 4 is replotted versus the loading rate. The loading rates used here were determined experimentally. For each loading

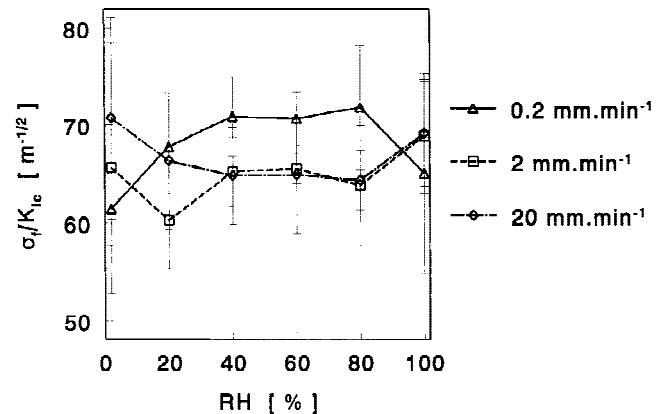


FIG. 7. Value of \mathcal{R} versus relative humidity at three loading rates for type-4 material.

rate, the fracture toughness increases with decreasing humidity. The fit procedure based on the SCG power law [Eq. (41)] was used on the data of core type 4, calculating the SCG parameter, n , assumed not to vary with humidity, and different values for the adsorption-controlled fracture toughness, \hat{K}_{Ic} and the pre-exponential factor, $v_{p_{H_2O}}$, for different humidities. The resulting values are given in Table II.

Figure 9 shows the adsorption-controlled fracture toughness resulting from the fit to the SENB results and resulting directly from the DT tests. The inert fracture toughness, as measured in vacuum, is also shown.

The dependence of the adsorption-controlled fracture toughness on the relative humidity can be described using Eq. (13) and the parameter b_{H_2O} from the measured adsorption isotherm ($b_{H_2O} = 0.71$). The values found for the different resulting fit parameters are listed in Table III and IV. The value for the inert fracture toughness determined from the fit on the SENB data, as $2.0 \text{ MPa m}^{1/2}$, agrees very well with the value of $1.99 \text{ MPa m}^{1/2}$ determined experimentally in high vacuum. The fit on fracture toughness obtained in this way turns out to be of a good quality.

Comparing the adsorption-controlled fracture toughness determined from the SCG fit to the SENB results and measured directly using the DT test shows that the effects of humidity on adsorption-controlled fracture toughness can be contributed to the decrease in fracture surface energy by adsorption.

The crack growth rate depends on the water partial pressure in two ways, as can be seen from Eqs. (27) and (26). The factor $v_{\eta} = p_{H_2O}^{\eta}$ accounts for the kinetic effect of water vapor pressure on the reaction rate. According to the standard chemical reaction rate theory, the extent of its influence depends on the (pseudo-) reaction order, η . The factor

$$v_{ads} = (1 + bp_{H_2O})^{n\Phi/2}, \quad (50)$$

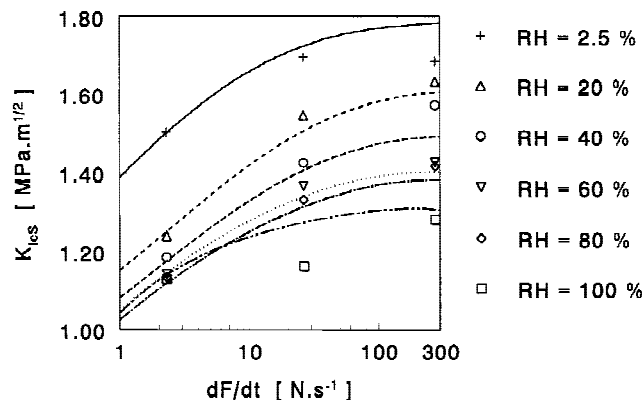


FIG. 8. SCG power law fit to experimental fracture toughness data for type-4 material versus loading rate.

accounts for the effect of adsorption on fracture surface energy and therefore, indirectly, crack growth rate. As the latter effect has been characterized successfully by measuring the water adsorption isotherm and by determining the adsorption-controlled fracture toughness in two independent ways, the kinetic effect of water vapor pressure on the crack growth rate can be obtained from

$$v_0 p_{H_2O}^{\eta} = \frac{v_{p_{H_2O}}}{v_{ads} \sqrt{1 - \Phi \ln(1 + bp_{H_2O})^n}}. \quad (51)$$

Using the values for the parameters as obtained in this analysis up to now, the factor $v_0 p_{H_2O}^{\eta}$ can be calculated. The resulting values are plotted in Fig. 10. Standard deviations are typically on the order $1 \times 10^{-4} \text{ m s}^{-1}$. For

TABLE II. Values of fit parameters determined assuming the fracture toughness to depend on relative humidity.

RH (%)	\hat{K}_{Ic} (MPa m ^{1/2})	n (-)	$v_{p_{H_2O}}$ (10 ⁻⁴ m/s)
2.5	1.792	11.73	1.953
20	1.624	11.73	8.237
40	1.508	11.73	7.268
60	1.416	11.73	5.316
80	1.396	11.73	5.262
100	1.317	11.73	2.299

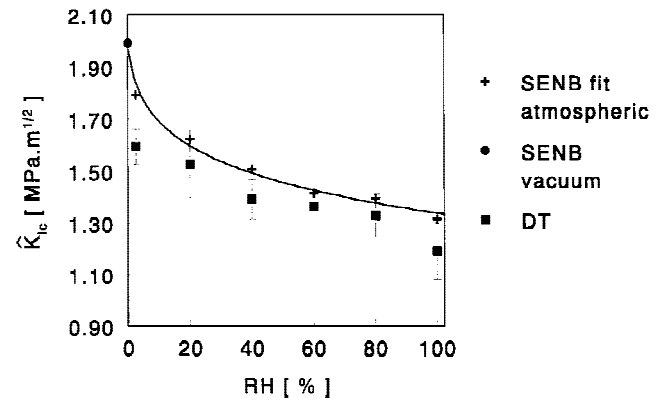


FIG. 9. Adsorption-controlled fracture toughness as measured using DT method for type-4 material and obtained from SCG power law fit and inert fracture toughness as measured using SENB test in vacuum.

TABLE III. Values of parameters found by fitting the adsorption equation to the fracture toughness data versus relative humidity, surface excess at full coverage calculated from fit data, and Langmuir constant b determined from adsorption isotherm experiments.

Parameter	Value
\hat{K}_{Ic} (MPa m ^{1/2})	1.97
Φ (-)	0.94
b (-)	0.71
Γ_M (10 ⁻⁴ mol m ⁻²)	6.26

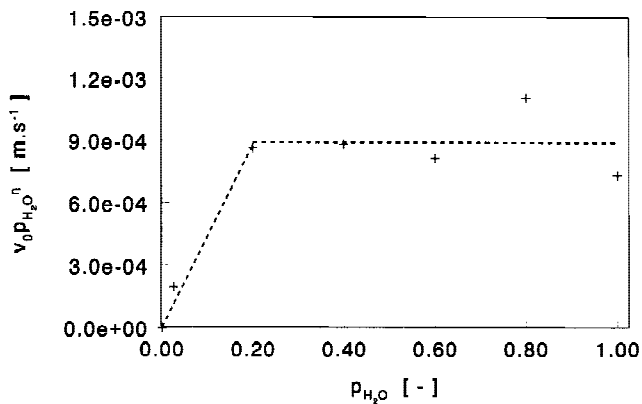


FIG. 10. Pre-exponential factor versus water vapor pressure.

$p_{\text{H}_2\text{O}} \leq 0.20$, $v_0 p_{\text{H}_2\text{O}}^{\eta}$ depends linearly on $p_{\text{H}_2\text{O}}$; that is, $\eta = 1$. This corresponds to a situation where one water molecule is responsible for breaking one bond. A mechanism as shown by states I–IIb–IIIb–IV in Fig. 1 can be envisaged for this situation. In this pressure range, $v_0 = 4.38 \times 10^{-3} \text{ m s}^{-1}$. At higher water vapor pressures ($p_{\text{H}_2\text{O}} \geq 0.20$), the factor $v_0 p_{\text{H}_2\text{O}}^{\eta}$ no longer depends on $p_{\text{H}_2\text{O}}$; that is, $\eta = 0$.

It is improbable that this is caused by a rate limitation in the bond-breaking reaction; as in catastrophic crack growth, higher crack growth rates can be reached. A mechanism where the actual breaking of the bond no longer depends on the formation of a transition state complex would limit the influence of the vapor molecules to a decrease in fracture energy by covering the fresh fracture surface (i.e., to adsorption). This corresponds to the reaction I–IIa–IIIa–IV in Fig. 1. The rate of the kinetic mechanism can be limited if the formation of the transition state complex is rate limiting. The adsorption residence time of a single adsorbate molecule is inversely proportional to the partial pressure. An increase in pressure will decrease the probability for a molecule to stay adsorbed long enough to form the transition state complex. Therefore, a limited contribution of this mechanism to SCG can be expected at higher pressures. On the other hand, at higher water vapor activities, the stress-enhanced thermal activation can become rate limiting. In that case, a sufficient supply of water is present, leading to a zeroth-order reaction in water.

TABLE IV. Values of fit parameters for the fracture toughness at separate loading rates as found using the measured adsorption isotherm.

v_{load} (mm min ⁻¹)	\tilde{K}_{Ic} (MPa m ^{1/2})	Φ (-)	Γ_{M} (10 ⁻⁴ mol m ⁻²)
0.2	1.80	0.62	4.80
2	2.14	0.64	5.81
20	1.99	0.47	3.39

The values of the factor $v_0 p_{\text{H}_2\text{O}}^{\eta}$ can be shown to be independent of the loading rate, by fitting as a function of loading rate, instead of humidity. This shows that the vapor pressure at the crack tip is equal to, or at least linear proportional to, the atmospheric bulk vapor pressure, meaning that no diffusion limitation of crack growth rate occurs.

Empirical power law models

A large number of empirical crack growth rate power laws have been used in the past to describe SCG. For example, a power law resembling Eq. (26) can be used with the inert fracture toughness and a humidity independent pre-exponential factor, v'_0 . The fit of the resulting relation to the data of core type 4 gives $n = 24$ and $v'_0 = 2.7 \times 10^{-3} \text{ m s}^{-1}$. As the factor $v_{\text{ads}} p_{\text{H}_2\text{O}}^{\eta}$ is about constant for $p_{\text{H}_2\text{O}} \geq 0.20$, this power law can be used in this humidity range, but the fit parameters have no physical relevance.

A number of similar power laws have been proposed with a humidity-dependent pre-exponential factor, according to $v'_0 = v''_0 p_{\text{H}_2\text{O}}^{\eta}$. A review of the application of such power laws to SCG in optical fibers generally showed a reaction order, η , of 2.5.^{18–21} Using this to model the fracture toughness data of core type 4 results in $\eta = 2.99$, while the pre-exponential factor, v''_0 , differs with a factor of 19 from the value resulting from our SCG analysis. For this type of empirical power law an effective reaction order η' can be determined for which applies

$$v'_0 p_{\text{H}_2\text{O}}^{\eta'} = v_0 p_{\text{H}_2\text{O}}^{\eta} (1 + b p_{\text{H}_2\text{O}})^{n\Phi/2} \quad (52)$$

For $b p_{\text{H}_2\text{O}} \gg 1$, it applies that $v'_0 = v_0 b^{n\Phi/2}$ and $\eta' = \eta + n\Phi/2$. This shows that, thanks to its mathematical similarity to Eq. (26), this type of power law model can be used to describe the fracture toughness, but that its success is rather fortuitous.

IX. CORRESPONDENCE BETWEEN FRACTURE TOUGHNESS AND STRENGTH

In this section, it will be shown that the changes in strength of material types 2 and 4 with changing humidity and stressing rate, as shown in Figs. 6 and 7, correspond to the respective changes in fracture toughness as measured in SENB tests. As some of the humidities at which the strength of material type 2 was measured differ from those at which the fracture toughness was determined, the strength data were linearly interpolated to the corresponding humidities.

The ratio $\mathcal{R} = K_{\text{Ic}}/\sigma_f$ can be calculated for each combination of stressing rate and relative humidity, from the available strength and the fracture toughness data, using Eq. (45). In order to check whether the ratio between

actual fracture toughness and actual strength is really constant, this ratio was calculated for both material types 2 and 4. Therefore, the null hypothesis that the individual means of \mathcal{R} taken for each particular combination of stressing rate and humidity, $\mu(\mathcal{R})$, are all statistically the same as the overall-mean of all separate values of \mathcal{R} , denoted as $\bar{\mathcal{R}}$. So, the null hypothesis can be formulated as $H_0: \mu(\mathcal{R}) = \mu(\bar{\mathcal{R}})$, which will be tested against the alternative hypothesis $H_1: \mu(\mathcal{R}) \neq \mu(\bar{\mathcal{R}})$.²² After calculating the standard deviation and the number of degrees of freedom of \mathcal{R} , the parameter t can now be calculated from

$$t = \frac{\bar{\mathcal{R}} - \mathcal{R}}{sp \sqrt{\frac{1}{n(\bar{\mathcal{R}})} + \frac{1}{n(\mathcal{R})}}}, \quad (53)$$

using the combined unbiased estimate of the sample standard deviation, sp , given by²²

$$sp = \sqrt{\frac{[n(\bar{\mathcal{R}}) - 1] \text{s.d.}(\bar{\mathcal{R}})^2 + [n(\mathcal{R}) - 1] \text{s.d.}(\mathcal{R})^2}{\nu(\bar{\mathcal{R}}) + \nu(\mathcal{R})}}. \quad (54)$$

Choosing the significance level at $\alpha = 0.005$, one finds for a two-tailed test, with a number of degrees of freedom, $\nu = 17$, a critical value for the test statistic $t_{\alpha, \nu}$ of 2.898 (which means that $P(|t|) > 2.898 = 1\%$).

The number of samples in the strength tests, $n(\bar{\sigma}_f)$ was 25 for all tests. The resulting values of t show that at only 3 out of 18 test conditions, the null hypothesis has to be rejected (at 0.2 mm min⁻¹, 2.5% RH and 60% RH and at 2 mm min⁻¹, 20% RH). The values of \mathcal{R} are shown in Figs. 6 and 7. the overall mean of \mathcal{R} for material type 2 is 38.74 m^{-1/2}; for material type 4 it is 66.52 m^{-1/2}.

Using the defect geometry factors $Y_S = 1.85$ and $Y = 1.26$, corresponding to $c_0 \approx 100 \mu\text{m}$ and $c_i \approx 600 \mu\text{m}$, for the initial notch in a SENB specimen and a half-penny shaped defect in a bending test, respectively, the last factor of the right-hand side of Eq. (45) is about 1.2 for all realistic values of the parameters.

Using Eq. (45) to calculate the mean initial sizes of the defects in material types 2 and 4 results in approximately 290 μm and 100 μm , using $Y = 1.26$, assuming a semi-circular crack shape. These are somewhat larger than the actual sizes of the critical defects as observed in these materials by fractography.¹ Comparing the results of material types 2 and 4 shows that the type and geometry of the defects (processing-induced cannibalistic grains or large pores in case of material type 2, and grinding damage in material type 4) do not influence the sensitivity to humidity, nor does the geometry of the specimen have any influence. Apart from the conclusion that the experiments were performed accurately, using appropriate methods, these results show that fracture toughness

measurements can be used to characterize the effect of humidity on the mechanical reliability of a material, instead of using much larger series of strength tests, or methods with restrictions as to the minimum sample size, like double torsion tests. Finally, the SCG model introduced here to describe the environmental effects on the fracture toughness equally applies to the effects on strength.

X. FRACTOGRAPHY

From the observation that the fraction transgranular fracture ranged between ~60% (high RH, low rate) to ~40% (low RH, high rate), we conclude that SCG favors transgranular fracture. This agrees with the observations as reported by Beauchamp and Monroe.²⁴ Since the amount of transgranular fracture for the strength specimens decreases with crack extension, we note that the effective humidity at the crack tip is influenced by the humidity in the environment and by the limited diffusion to the crack tip.

Crack bridging was observed but only rarely and is thus much less pronounced as reported before.²⁴ Consequently, crack bridging is neglected in the model. Beauchamp and Monroe²⁴ also report a change from about 85% to 50% transgranular fracture as a function of stress intensity, more or less independent of RH. It should be remarked though, that significant differences in materials are present, both in composition and grain size. Compare: this work, 71.0 wt% Fe₂O₃, 20.5 wt% MnO, and 8.5 wt% ZnO versus ~63 wt% Fe₂O₃, ~25 wt% MnO, and ~11 wt% ZnO of Beauchamp and Monroe²⁴; and this work, 7.3 μm versus 24 and 35 μm of Beauchamp and Monroe,²⁴ all linear intercept measurements. A change in fracture mode ratio was also reported in Ref. 25 but unfortunately only qualitative changes and no material details were presented.

XI. CONCLUSIONS

In this paper, it is shown that fracture toughness measurements performed on MnZn ferrites are affected by environmental humidity. The SCG power law, incorporating the chemical activity of the reactive species and the surface energy decrease caused by adsorption of those species on the fracture surface, was successfully used to describe the dependence of actual fracture toughness on humidity and loading rate. The adsorption-controlled fracture toughness and the pre-exponential factor from this model were both determined by a fit of the model to the experimental data. The adsorption-controlled fracture toughness was also measured directly, using the double torsion method. From the dependence of the pre-exponential factor on the humidity, it was shown

that for small water vapor pressures ($p_{\text{H}_2\text{O}} \leq 0.20$), the reaction order, η , is unity while for larger humidities $\eta = 0$. A tentative explanation for this effect has been given, based on a decreasing adsorption time, compared to the time needed to form a transition state complex after adsorption. Perhaps the stress-enhanced thermal equilibrium kinetics become rate limiting. It has been shown that for higher humidities, empirical rate laws used “traditionally” can be successful as well. Their success is, however, fortuitous and relies only on the mathematical similarity between the resulting relations. The results of the SENB fracture toughness tests are shown to be equivalent to those of the W strength tests. The effects of SCG are independent of the type or size of the initial defects. Therefore, to characterize the mechanical reliability of an MnZn ferrite and the effects of SCG, SENB tests can be used, with the advantage that a smaller number of tests has to be performed.

REFERENCES

1. M. Donners, L. Dortmans, G. de With, and M. de Graaf, *J. Eur. Ceram. Soc.* **17**, 1591 (1997).
2. M. Donners, G. de With, and J. Niemantsverdriet (unpublished).
3. A.W. Adamson, *Physical Chemistry of Surfaces* (Interscience Publishers, New York, 1967).
4. J-C. Pollet and S.J. Burns, *Int. J. Fract.* **13**, 667 (1977).
5. A.S. Krausz and K. Krausz, *Fracture Kinetics of Crack Growth* (Kluwer Academic Publishers, Dordrecht, 1988).
6. S. Glasstone, K.J. Laidler, and H. Eyring, *The Theory of Rate Processes* (McGraw-Hill, New York, 1941).
7. B. Lawn, *Fracture of Brittle Solids*, Second edition (Cambridge University Press, Cambridge, United Kingdom, 1993).
8. J.E. Srawley, *Int. J. Fract.* **12**, 475 (1976).
9. W.F. Brown and J.E. Srawley, *ASTM Spec. Tech. Publ.* **410**, 12 (1966).
10. E.R. Fuller, *ASTM Spec. Tech. Publ.* **678**, 3 (1979).
11. B.J. Pletka, E.R. Fuller, and B.G. Koepke, *ASTM Spec. Tech. Publ.* **678**, 19 (1979).
12. D.P. Williams and A.G. Evans, *J. Test. Eval.* **1**, 264 (1973).
13. A.V. Virkar and D.L. Johnson, *J. Am. Ceram. Soc.* **59**, 197 (1976).
14. J.G. Bruce and B.G. Koepke, *J. Am. Ceram. Soc.* **60**, 284 (1977).
15. L. Li, J.M. Weick, and R.F. Pabst, *Ber. Dt. Keram. Ges.* **57**, 5 (1980).
16. O. Kadouch, Ph.D. Thesis, ENSR Paris, France (1993).
17. R.F. Pabst and J.M. Weick, *J. Mater. Sci. Lett.* **16**, 836 (1981).
18. W.J. Duncan, K.J. Beales, D.M. Cooper, P.L. Dunn, M. Herman, J.D. Rush, and G.R. Thomas, in *Fiber Optics in Adverse Environments* (Proceedings of SPIE, Bellingham, WA, 1984), Vol. 2 pp. 134–138.
19. J.L. Armstrong, M.J. Matthewson, and C.R. Kurkjian, in *Abstract Book, 100th Annual Meeting, American Ceramic Society, Abstract SXVII-004-98* (1998).
20. S. Sakaguchi and T. Kimura, *J. Am. Ceram. Soc.* **64**, 259 (1981).
21. M. Muraoka, K. Ebata, and H. Abé, *J. Am. Ceram. Soc.* **76**, 1545 (1993).
22. A.M. Mood, F.A. Graybill, and D.C. Boes, *Introduction to the Theory of Statistics*, 3rd ed. (McGraw-Hill, New York, 1974).
23. P.S. Leerers, *J. Mater. Sci.* **17**, 2469 (1982).
24. E.K. Beauchamp and S.L. Monroe, *J. Am. Ceram. Soc.* **72**, 1179 (1989).
25. H. Takahashi, H. Iwaya, and T. Yamasaki, in *Ferrites*, Proceedings of the 6th International Conference on Ferrites (ICF6) (The Japan Society of Powder and Powder Metallurgy, Tokyo, 1992, p. 309).